# (Hf0.2Zr0.2Ta0.2Nb0.2Ti0.2)C high-entropy ceramics with low thermal conductivity

Xueliang Yan, Loic Constantin, Yongfeng Lu, Jean-François Silvain, Michael Nastasi, Bai Cui

PROFESSOR BAI CUI (Orcid ID : 0000-0002-0585-6698)



Article type : Rapid Communication

# $(Hf_{0.2}Zr_{0.2}Ta_{0.2}Nb_{0.2}Ti_{0.2})C$ High-Entropy Ceramics with Low Thermal Conductivity

Xueliang Yan[‡], Loic Constantin[§,¦], Yongfeng Lu[§], Jean-François Silvain[¦], Michael Nastasi[‡,¶,‖], Bai Cui[‡,‖,*,†]

[‡] Department of Mechanical & Materials Engineering, University of Nebraska–Lincoln, Lincoln, NE 68588, USA

[§] Department of Electrical Engineering, University of Nebraska–Lincoln, Lincoln, NE 68588, USA

[¦] Institut de Chimie de la Matière Condensée de Bordeaux – ICMCB-CNRS 87, Avenue du Docteur Albert Schweitzer, F-33608 Pessac Cedex, France

[¶] Nebraska Center for Energy Sciences Research, University of Nebraska–Lincoln, Lincoln, NE 68588, USA

[†]Corresponding author. Tel.: +1 (402) 472-5740; fax: +1 (402) 472 1465; email: bcui3@unl.edu.

[*]Member, American Ceramic Society.

This is the author manuscript accepted for publication and has undergone full peer review but has not been through the copyediting, typesetting, pagination and proofreading process, which may lead to differences between this version and the Version of Record. Please cite this article as doi: 10.1111/jace.15779

[I] Nebraska Center for Materials and Nanoscience, University of Nebraska-Lincoln, Lincoln, NE, 68588, USA



## Abstract

A novel high-entropy carbide ceramic, $(Hf_{0.2}Zr_{0.2}Ta_{0.2}Nb_{0.2}Ti_{0.2})C$, with a single-phase rock salt structure, was synthesized by spark plasma sintering. X-ray diffraction confirmed the formation of a single-phase rock salt structure at 26-1140 °C in Argon atmosphere, in which the five metal elements likely share a cation position while the C element occupies the anion position. $(Hf_{0.2}Zr_{0.2}Ta_{0.2}Nb_{0.2}Ti_{0.2})C$ exhibits a much lower thermal diffusivity and conductivity than the five binary carbides HfC, ZrC, TaC, NbC and TiC, which may result from the significant phonon scattering at its distorted anion sublattice. $(Hf_{0.2}Zr_{0.2}Ta_{0.2}Nb_{0.2}Ti_{0.2})C$ inherits the high elastic modulus and hardness of the binary carbide ceramics.

**Keywords**: high-entropy ceramics, microstructure, thermal conductivity, spark plasma sintering

## 1. Introduction

In the last decade, metallic high-entropy alloys (HEAs) have attracted extensive research interest.[1] Unlike traditional metal alloys, HEAs contain four or more metal

elements in equal or near-equal atomic percentage, but form a single-phase solid solution with simple lattice structures (such as body-centered cubic or face-centered cubic) due to a high configuration entropy.[2, 3] Because the minimization of Gibbs free energy ($G = H-TS$, where $H$ is enthalpy, $S$ is entropy, and $T$ is temperature) controls the thermodynamic stability of a material, high-entropy materials with a large $S$ can be more thermodynamically stable at high temperatures. In addition, high-entropy materials have shown superior mechanical properties, corrosion resistance, thermal properties, and irradiation tolerance to traditional materials.[3, 4, 5]

Compared to metallic HEAs, very few high-entropy ceramics (HECs) have been discovered. High-entropy ceramics are characterized by an intrinsic atomic disorder of metal elements in the cation position, resulting in compositional complexity and significant lattice distortion. The high configuration entropy may make the HECs more thermodynamically stable at high temperatures. Rose *et al*. first reported a high-entropy oxide, $(Mg_{0.2}Co_{0.2}Ni_{0.2}Cu_{0.2}Zn_{0.2})O$ prepared by quenching, which has a single-phase rock salt structure.[6] Later, Bérardan *et al*. found that this oxide and its derivatives, $(Mg_{0.2}Co_{0.2}Ni_{0.2}Cu_{0.2}Zn_{0.2})_{1-x-y}A_xGa_yO$ (where A = Li, Na or K), exhibit colossal dielectric constants[7] and superionic conductivity.[8] Gild *et al*. synthesized a family of high-entropy borides, including $(Hf_{0.2}Zr_{0.2}Ta_{0.2}Nb_{0.2}Ti_{0.2})B_2$ and $(Hf_{0.2}Zr_{0.2}Ta_{0.2}Mo_{0.2}Ti_{0.2})B_2$, by spark plasma sintering (SPS). These high-entropy borides exhibit a single-phase solid solution with a layered hexagonal structure, and show higher hardness and oxidation resistance than the binary metal diborides such as $HfB_2$ or $ZrB_2$.[9] Despite these recent studies, little is known about the mechanisms associated with the underlying atomic disorder in the HECs, which controls their microstructures and properties.

This paper presents the synthesis, microstructures, and properties of a novel high-entropy carbide ceramic, $(Hf_{0.2}Zr_{0.2}Ta_{0.2}Nb_{0.2}Ti_{0.2})C$. X-ray diffraction (XRD) confirmed the formation of a single-phase rock salt structure (space group $Fm\bar{3}m$), in which the five metal elements (Hf, Zr, Ta, Nb, and Ti) may share a cation position

while the C element occupies the anion position. The $(Hf_{0.2}Zr_{0.2}Ta_{0.2}Nb_{0.2}Ti_{0.2})C$ exhibits low thermal conductivity and diffusivity, which is much lower than the five binary carbides HfC, ZrC, TaC, NbC and TiC. In addition, $(Hf_{0.2}Zr_{0.2}Ta_{0.2}Nb_{0.2}Ti_{0.2})C$ inherits the high elastic modulus and hardness of the binary carbide ceramics. These excellent properties make high-entropy carbide ceramics as a promising candidate for thermal insulation materials in aeronautic and automotive applications such as spacecraft and gas turbines.

## 2. Experimental

High-entropy carbide ceramics, $(Hf_{0.2}Zr_{0.2}Ta_{0.2}Nb_{0.2}Ti_{0.2})C$, were synthesized by spark plasma sintering (SPS). Commercially available HfC (99.5%, <45 µm powder size), ZrC (99.5%, <45 µm), TaC (99.5%, <45 µm), NbC (99.0%, <45 µm), and TiC (99.5%, <45 µm) were purchased from Alfa Aesar. These powders, with an equimolar composition (HfC: ZrC: TaC: NbC: TiC=1:1:1:1:1), were mixed in a glove box under an Ar atmosphere to avoid oxidation. The powders were added into a 316-stainless steel grinding bowl for ball milling in an Ar atmosphere (1 atm). The grinding balls are 10 mm in diameter and the ball-to-powder mass ratio was 5:1. The mixture of powders was milled at 250 rpm for 6 h using a high-energy planetary ball mill (Model Pulverisette 7, Fritsch GmbH). To prevent overheating, ball milling was interrupted for 5 min, every 60 min for cooling. Consolidation of the ball milled powders was performed in an SPS system (Model SPS 10-4, Thermal Technologies) in a vacuum ($2\times10^{-2}$ Torr) at 2000 °C for 5 min under a pressure of 30 MPa. The heating rate was 100 °C/min. A 25µm-thick molybdenum foil was used to separate the powders from the graphite die to prevent a reaction between them. The synthesized samples' diameter and thickness were about 20 mm and 1 mm, respectively.

The phase composition in the as-sintered sample was characterized by XRD using a diffractometer (AXS D8 Discover, Bruker) with Cu $K_\alpha$ radiation. Jade software (V6.2, Materials Data Inc.) was used to refine the lattice parameters from XRD peaks. To examine the thermal stability of the high entropy ceramics, the as-sintered $(Hf_{0.2}Zr_{0.2}Ta_{0.2}Nb_{0.2}Ti_{0.2})C$ samples were annealed at 500, 800 and 1140 °C for 1 hour in Argon atmosphere. After annealing, the samples were characterized by XRD with Cu $K_\alpha$ radiation.

The microstructures were characterized by a FIB/SEM dual-beam workstation (Helios 660 NanoLab, FEI) using the secondary electron imaging mode. The grain size was statistically measured from the fracture surface for over 100 grains using ImageJ software (Version 1.51f, National Institute of Health). The chemical element distribution was analyzed by energy dispersive X-ray spectroscopy (EDS) using an EDS system (Octane Super, EDAX) equipped in the Helios 660.

The density of the as-sintered sample was measured using the Archimedes method on a balance (AT201, Mettler Toledo). The theoretical density of $(Hf_{0.2}Zr_{0.2}Ta_{0.2}Nb_{0.2}Ti_{0.2})C$ was calculated from the mass of the atoms in a unit cell and the lattice parameters measured from the XRD data. The Young's modulus ($E$) was calculated using the nanoindentation load-displacement curve measured in a triboindenter (TI 950, Hysitron), following the method developed by Oliver and Pharr.[10] The Vickers microhardness ($H_v$) was measured using a hardness tester under a load of 9.8 N and a dwell time of 10 seconds (Tukon 2500, Wilson).

Thermal conductivity ($k$) was calculated from the thermal diffusivity ($\alpha$), density ($\rho$), and specific heat ($c_p$) according to the following equation:

$$k = \alpha \rho c_p \quad (1)$$

Thermal diffusivity was measured using a laser flash unit (LFA 457/2/G microflash, Netzsch). The sample was coated with a light spray of graphite to prevent any undesirable reflection of the laser beam. The thermal diffusivity measurements were performed under air atmosphere and from 15 laser shots. Specific heat capacity was

measured on a differential scanning calorimeter (DSC 204 F1 Phoenix, Netzsh).[11] The linear thermal expansion was measured using a dilatometer (402C, Netzsch) in Ar atmosphere from 25 to 300 ºC at heating and cooling rates of 3 ºC/min. The thermal expansion coefficient ($\alpha_L$) was calculated from linear thermal expansion.

## 3. Results and discussion

**Fig. 1a** shows the XRD spectrum of $(Hf_{0.2}Zr_{0.2}Ta_{0.2}Nb_{0.2}Ti_{0.2})C$, which is compared with those of the five binary carbides used in its synthesis (HfC, ZrC, TaC, NbC and TiC). The XRD peaks suggest a single-phase of a rock-salt structure (space group $Fm\bar{3}m$), which is the same structure as the five binary carbides. It is important to note that ball-milled powders were still a mixture of HfC, ZrC, TaC, NbC and TiC, while a single phase ($Hf_{0.2}Zr_{0.2}Ta_{0.2}Nb_{0.2}Ti_{0.2}$) was formed after sintering by SPS.

Based on the XRD data, the schematic diagram of the rock salt structure of $(Hf_{0.2}Zr_{0.2}Ta_{0.2}Nb_{0.2}Ti_{0.2})C$ is presented in **Fig. 1b**. It is noted that this is a simplified schematic diagram that does not take the lattice distortion into account. The five metal elements (Hf, Zr, Ta, Nb, and Ti) very likely share a cation position, while the C element occupies the anion position. The thermal stability of $(Hf_{0.2}Zr_{0.2}Ta_{0.2}Nb_{0.2}Ti_{0.2})C$ was studied by the annealing experiments. After annealing at 500, 800 and 1140 °C for 1 hour under argon environment, the XRD spectra showed no evidence of phase decomposition or transformation, indicating that the high-entropy phase $(Hf_{0.2}Zr_{0.2}Ta_{0.2}Nb_{0.2}Ti_{0.2})C$ is thermally stable up to 1140 °C (**Fig. 1c**).

The lattice parameter *a* of $(Hf_{0.2}Zr_{0.2}Ta_{0.2}Nb_{0.2}Ti_{0.2})C$ was calculated to be 4.5180 Å, which is close to the average lattice parameter (4.5130 Å) of the five binary carbides (**Table 1**). In the high-entropy ceramics, the rearrangement of the multiple metallic elements can generate distinction in lattice parameters, which transfer the sub-lattice into an unstandardized rock-salt structure. Due to the lattice distortion in

this unstandardized rock-salt structure, the lattice parameter of $(Hf_{0.2}Zr_{0.2}Ta_{0.2}Nb_{0.2}Ti_{0.2})C$ is just an average estimation. The theoretical density of $(Hf_{0.2}Zr_{0.2}Ta_{0.2}Nb_{0.2}Ti_{0.2})C$ is 9.385 g/cm$^3$ , which is calculated from its lattice parameter and is an average estimation. The measured density of the bulk $(Hf_{0.2}Zr_{0.2}Ta_{0.2}Nb_{0.2}Ti_{0.2})C$ sample using the Archimedes method was 8.751 g/cm$^3$, suggesting the relative density of the bulk sample is 93%.

The SEM micrographs of a typical fracture surface of the $(Hf_{0.2}Zr_{0.2}Ta_{0.2}Nb_{0.2}Ti_{0.2})C$ sample (**Fig. 2a**) revealed uniaxial grains with an average grain size of 16.4 ± 4.5 µm. The SEM image of the polished surface and the corresponding EDS mapping of Hf, Zr, Ta, Nb and Ti elements are shown in **Fig. 2b**. The distribution of these metal cation elements is homogeneous at the micrometer level, indicating that these metal elements formed a solid solution. No element degradation was identified from the EDS mapping, confirming that a single phase is present in the $(Hf_{0.2}Zr_{0.2}Ta_{0.2}Nb_{0.2}Ti_{0.2})C$ sample. The TEM images of $(Hf_{0.2}Zr_{0.2}Ta_{0.2}Nb_{0.2}Ti_{0.2})C$ show uniaxial grains with a grain size of 10-20 µm.

The thermal properties of $(Hf_{0.2}Zr_{0.2}Ta_{0.2}Nb_{0.2}Ti_{0.2})C$ measured are listed in **Table 2** and compared with those of the five binary carbides HfC, ZrC, TaC, NbC and TiC. The $(Hf_{0.2}Zr_{0.2}Ta_{0.2}Nb_{0.2}Ti_{0.2})C$ shows a very low thermal diffusivity (3.6 mm$^2$/s) at 29.5 °C, which is 57% of the lowest value (6.29 mm$^2$/s) in the five binary compounds at room temperature (25 °C). As a result, $(Hf_{0.2}Zr_{0.2}Ta_{0.2}Nb_{0.2}Ti_{0.2})C$ exhibits a low thermal conductivity, 6.45 W/m·K at 29.5 °C, which is less than one-fourth of the thermal conductivity of the binary compounds of ultra-high-temperature ceramics (UHTCs) such as HfC (29.3 W/m·K) or TaC (33.5 W/m·K) and is only comparable to the thermal conductivity of NbC (6.3 W/m·K) at room temperature. With increasing temperature, the thermal conductivity of $(Hf_{0.2}Zr_{0.2}Ta_{0.2}Nb_{0.2}Ti_{0.2})C$ decreases to 5.42 W/m·K at 70.8 °C. In addition, the thermal expansion coefficient of $(Hf_{0.2}Zr_{0.2}Ta_{0.2}Nb_{0.2}Ti_{0.2})C$ is $6.44\times10^{-6}$ K$^{-1}$ at 25 °C,

which is comparable to that of the five binary carbides (HfC, ZrC, TaC, NbC and TiC) (**Table 2**).

The low thermal conductivity of $(Hf_{0.2}Zr_{0.2}Ta_{0.2}Nb_{0.2}Ti_{0.2})C$ may result from the high-entropy effects. Phonons and electrons are the main carriers for transferring heat in solids. For transition metal carbides, such as TiC, the electron contribution accounts for about 25% of the total heat conduction at room temperature, as estimated from the Wiedemann-Franz law, leaving the phonon contribution at about 75%.[21] When HfC, ZrC, TaC, NbC, and TiC form the high-entropy phase $(Hf_{0.2}Zr_{0.2}Ta_{0.2}Nb_{0.2}Ti_{0.2})C$, the phonon contribution may be changed much while the electron contribution is not. Due to the different sizes and bonding strengths of the five individual metal atoms (Hf, Zr, Ta, Nb and Ti) in the cation positions, there exist significant atomic-scale lattice distortions for the lattice sites in $(Hf_{0.2}Zr_{0.2}Ta_{0.2}Nb_{0.2}Ti_{0.2})C$. Recently, Rost et al. present an extended X-ray absorption fine structure (EXAFS) analysis of an HEC, $(Mg_{0.2}Co_{0.2}Ni_{0.2}Cu_{0.2}Zn_{0.2})O$.[22] It showed that the crystal models that best fit the experimental X-ray scatting data are cations that are distributed randomly on an FCC sublattice with minimum positional disorder, with an interleaved anion FCC sublattice in which oxygen ions are displaced from the ideal locations to accommodate the distortions in the cation polyhedral. In $(Mg_{0.2}Co_{0.2}Ni_{0.2}Cu_{0.2}Zn_{0.2})O$, the distortion from an ideal rock-salt structure occurs primarily through the disorder in the anion sublattice. Because $(Hf_{0.2}Zr_{0.2}Ta_{0.2}Nb_{0.2}Ti_{0.2})C$ has a similar rock-salt structure with $(Mg_{0.2}Co_{0.2}Ni_{0.2}Cu_{0.2}Zn_{0.2})O$, it can be hypothesized that in $(Hf_{0.2}Zr_{0.2}Ta_{0.2}Nb_{0.2}Ti_{0.2})C$, the lattice distortion may also occur mainly through the anion sublattice. However, an EXAFS analysis will be needed to examine this hypothesis. In contrast to perfect crystals and ordered materials, the mass and interatomic force constant fluctuations in HECs, due to anion sublattice distortion, can induce severe phonon scattering.[23] The low thermal conductivity due to lattice distortion has also been observed in some other HEAs, such as PbSnTeSe and

$BiSbTe_{1.5}Se_{1.5}$.[24, 25, 26] The low thermal conductivity of $(Hf_{0.2}Zr_{0.2}Ta_{0.2}Nb_{0.2}Ti_{0.2})C$ may be mainly attributed to its distorted anion sublattice, at which the phonons are scattered more significantly. However, there is a significant difference in HECs and HEAs. In HECs such as $(Hf_{0.2}Zr_{0.2}Ta_{0.2}Nb_{0.2}Ti_{0.2})C$, the lattice distortion may occur mainly through the anion sublattice. In the HEAs such as PbSnTeSe, the lattice distortion exist in the whole crystal structure. In HEAs such as NiCoFeCr, it is suggested that an increasing number of principal elements and/or concentrations of specific elements can result in a substantial reduction in the electron mean free path and a decrease in electrical and thermal conductivity. The subsequently slow energy dissipation can affect the defect dynamics at the early stages, which may lead to less irradiation defects and improved irradiation resistance.[27, 28] It is thus possible that HECs such as $(Hf_{0.2}Zr_{0.2}Ta_{0.2}Nb_{0.2}Ti_{0.2})C$ may also show high irradiation tolerance similar to HEAs.

$(Hf_{0.2}Zr_{0.2}Ta_{0.2}Nb_{0.2}Ti_{0.2})C$ inherits the high elastic modulus and hardness of the binary carbides. The elastic modulus and Vickers hardness of $(Hf_{0.2}Zr_{0.2}Ta_{0.2}Nb_{0.2}Ti_{0.2})C$ are comparable to the five binary carbides HfC, ZrC, TaC, NbC and TiC (**Table 1**). The high elastic modulus and hardness of the transition metal carbides, such as HfC, have been attributed to their strong covalent metal-carbon bonds.[29] The local bond lengths of each cation-anion pair in $(Hf_{0.2}Zr_{0.2}Ta_{0.2}Nb_{0.2}Ti_{0.2})C$ may vary around each cation.[22] Therefore, it may need a quantitative EXAFS analysis of the local bond lengths of each cation-anion pair in $(Hf_{0.2}Zr_{0.2}Ta_{0.2}Nb_{0.2}Ti_{0.2})C$ to better correlate with the mechanical properties.

The beneficial effects of high entropy in carbide ceramics have been revealed in this study, i.e., thermal conductivities are decreased while the high elastic modulus and hardness can be retained. These material properties are important for aeronautic and automotive applications such as spacecraft and gas turbines. Such properties cannot be easily achieved from other processing routes such as forming composites.

## 4. Conclusion

A novel high-entropy metal carbide, $(Hf_{0.2}Zr_{0.2}Ta_{0.2}Nb_{0.2}Ti_{0.2})C$, was synthesized by SPS. The crystal structure and phase composition were characterized by XRD, showing a single-phase rock salt structure (space group $Fm\bar{3}m$), in which the five metal elements (Hf, Zr, Ta, Nb, and Ti) likely share a cation position while the C element occupies the anion position. The high-entropy phase $(Hf_{0.2}Zr_{0.2}Ta_{0.2}Nb_{0.2}Ti_{0.2})C$ is thermally stable at least up to 1140 °C in Argon atmosphere. $(Hf_{0.2}Zr_{0.2}Ta_{0.2}Nb_{0.2}Ti_{0.2})C$ exhibits low thermal conductivity and diffusivity, which are much lower than those of the five binary carbides HfC, ZrC, TaC, NbC and TiC. The low thermal conductivity may result from the significant phonon scattering at its distorted anion sublattice. The elastic modulus and hardness of $(Hf_{0.2}Zr_{0.2}Ta_{0.2}Nb_{0.2}Ti_{0.2})C$ are comparable to those of the five binary carbides, which may be attributed to the strong covalent metal-carbon bonds.


### I. Acknowledgement

The authors would like to thank Prof. Bill Lee (Imperial College London) and the reviewers for helpful technical discussions. This work was partially supported by the Research Council Interdisciplinary Grant from the University of Nebraska-Lincoln. Manufacturing and characterization analyses were performed at the NanoEngineering Research Core Facility (part of the Nebraska Nanoscale Facility), which is partially funded from the Nebraska Research Initiative. The research was performed in part in the Nebraska Nanoscale Facility: National Nanotechnology Coordinated Infrastructure and the Nebraska Center for Materials and Nanoscience, which are supported by the National Science Foundation under Award ECCS: 1542182, and the Nebraska Research Initiative.

## References


1. Yeh JW, Chen SK, Lin SJ, Gan JY, Chin TS, Shun TT, et al. Nanostructured high-entropy alloys with multiple principal elements: novel alloy design concepts and outcomes. Adv Eng Mater. 2004;6:299-303.
2. Tsai M-H, Yeh J-W. High-entropy alloys: a critical review. Mater Res Lett. 2014;2:107-123.
3. Zhang Y, Zuo TT, Tang Z, Gao MC, Dahmen KA, Liaw PK, et al. Microstructures and properties of high-entropy alloys. Prog Mater Sci. 2014;61:1-93.
4. Egami T, Ojha M, Khorgolkhuu O, Nicholson DM, Stocks GM. Local electronic effects and irradiation resistance in high-entropy alloys. JOM. 2015;67:2345-2349.
5. Granberg F, Nordlund K, Ullah MW, Jin K, Lu C, Bei H, et al. Mechanism of radiation damage reduction in equiatomic multicomponent single phase alloys. Phys Rev Lett. 2016;116:135504.
6. Rost CM, Sachet E, Borman T, Moballegh A, Dickey EC, Hou D, et al. Entropy-stabilized oxides. Nat Commun. 2015;6:8485.
7. Bérardan D, Franger S, Dragoe D, Meena AK, Dragoe N. Colossal dielectric constant in high entropy oxides. Phys Status Solidi RRL. 2016;10:328-333.
8. Bérardan D, Franger S, Meena A, Dragoe N. Room temperature lithium superionic conductivity in high entropy oxides. J Mater Chem A. 2016;4:9536-9541.
9. Gild J, Zhang Y, Harrington T, Jiang S, Hu T, Quinn MC, et al. High-entropy metal diborides: a new class of high-entropy materials and a new type of ultrahigh temperature ceramics. Sci Rep. 2016;6:37946.
10. Oliver WC, Pharr GM. An improved technique for determining hardness and elastic modulus using load and displacement sensing indentation experiments. J Mater Res. 1992;7:1564-1583.
11. O'neill M. Measurement of specific heat functions by differential scanning

calorimetry. Anal Chem. 1966;38:1331-1336.

12. Sciti D, Guicciardi S, Nygren M. Densification and mechanical behavior of HfC and HfB2 fabricated by spark plasma sintering. J Am Ceram Soc. 2008;91:1433-1440.
13. Sciti D, Guicciardi S, Nygren M. Spark plasma sintering and mechanical behaviour of ZrC-based composites. Scripta Mater. 2008;59:638-641.
14. Acicbe RB, Goller G. Densification behavior and mechanical properties of spark plasma-sintered ZrC–TiC and ZrC–TiC–CNT composites. J Mater Sci. 2013;48:2388-2393.
15. Cedillos-Barraza O, Grasso S, Al Nasiri N, Jayaseelan DD, Reece MJ, Lee WE. Sintering behaviour, solid solution formation and characterisation of TaC, HfC and TaC–HfC fabricated by spark plasma sintering. J Eur Ceram Soc. 2016;36:1539-1548.
16. Jiang X, Zhao J, Jiang X. Correlation between hardness and elastic moduli of the covalent crystals. Comput Mater Sci. 2011;50:2287-2290.
17. Demirskyi D, Sakka Y, Vasylkiv O. High-temperature reactive spark plasma consolidation of TiB 2–NbC ceramic composites. Ceram Int. 2015;41:10828-10834.
18. Cheng L, Xie Z, Liu G, Liu W, Xue W. Densification and mechanical properties of TiC by SPS-effects of holding time, sintering temperature and pressure condition. J Eur Ceram Soc. 2012;32:3399-3406.
19. Wang Y-J, Li H-J, Fu Q-G, Wu H, Yao D-J, Wei B-B. Ablative property of HfC-based multilayer coating for C/C composites under oxy-acetylene torch. Appl Surf Sci. 2011;257:4760-4763.
20. Elliott RO, Kempter CP. Thermal expansion of some transition metal carbides. J Phys Chem. 1958;62:630-631.
21. Morelli DT. Thermal conductivity and thermoelectric power of titanium carbide single crystals. Phys Rev B. 1991;44:5453.

22. Rost CM, Rak Z, Brenner DW, Maria JP. Local structure of the $Mg_xNi_xCo_xCu_xZn_xO$ (x=0.2) entropy-stabilized oxide: An EXAFS study. J Am Ceram Soc. 2017;100:2732-2738.

23. Körmann F, Ikeda Y, Grabowski B, Sluiter MH. Phonon broadening in high entropy alloys. npj Comput Mater. 2017;3:36.

24. Tsai M-H. Physical properties of high entropy alloys. Entropy. 2013;15:5338-5345.

25. Fan Z, Wang H, Wu Y, Liu X, Lu Z. Thermoelectric high-entropy alloys with low lattice thermal conductivity. RSC Adv. 2016;6:52164-52170.

26. Fan Z, Wang H, Wu Y, Liu X, Lu Z. Thermoelectric performance of PbSnTeSe high-entropy alloys. Mater Res Lett. 2017;5:187-194.

27. Egami T, Guo W, Rack P, Nagase T. Irradiation resistance of multicomponent alloys. Metall Mater Trans A. 2014;45:180-183.

28. Zhang Y, Stocks GM, Jin K, Lu C, Bei H, Sales BC, et al. Influence of chemical disorder on energy dissipation and defect evolution in concentrated solid solution alloys. Nat Commun. 2015;6:8736.

29. Price DL, Cooper BR. Total energies and bonding for crystallographic structures in titanium-carbon and tungsten-carbon systems. Phys Rev B. 1989;39:4945.

## Figure Captions:

**Fig. 1**. (a) XRD of $(Hf_{0.2}Zr_{0.2}Ta_{0.2}Nb_{0.2}Ti_{0.2})C$ at room temperature, compared with the five binary carbides used in the synthesis (HfC, ZrC, TaC, NbC and TiC). (b) Schematic diagram of the rock-salt structure of $(Hf_{0.2}Zr_{0.2}Ta_{0.2}Nb_{0.2}Ti_{0.2})C$. (c) XRD of $(Hf_{0.2}Zr_{0.2}Ta_{0.2}Nb_{0.2}Ti_{0.2})C$ before and after annealing at 500, 800 and 1140 °C for 1 hour in Argon atmosphere..

**Fig. 2.** Microstructural characterization of $(Hf_{0.2}Zr_{0.2}Ta_{0.2}Nb_{0.2}Ti_{0.2})C$: (a) SEM image of the fracture surface; and (b) SEM image of the polished surface, with the corresponding EDS mapping of Hf, Zr, Ta, Nb and Ti elements.

## Tables:

**Table 1.** Comparison of the lattice parameters and mechanical properties of $(Hf_{0.2}Zr_{0.2}Ta_{0.2}Nb_{0.2}Ti_{0.2})C$ with binary carbides HfC, ZrC, TaC, NbC and TiC.

| Materials | Lattice parameter, $a$ (Å) | Theoretical density, $\rho$ (g/cm$^3$) | Elastic modulus, $E$ (GPa) | Vickers hardness, $H_v$ (GPa) |
|---|---|---|---|---|
| **$(Hf_{0.2}Zr_{0.2}Ta_{0.2}Nb_{0.2}Ti_{0.2})C$** | 4.5180 | 9.385 | 479 | 15 |
| HfC | 4.641 | 12.6 | 450-500[12] | 18.3[12] |
| ZrC | 4.683 | 6 | 464[13] | 17.6[14] |
| TaC | 4.454 | 7.6 | 458[15] | 13.9[15] |
| NbC | 4.4691 | 4.56 | 392[16] | 22.1[17] |
| TiC | 4.3178 | 14 | 448[16] | 21.87[18] |

**Table 2.** Comparison of the thermal properties of $(Hf_{0.2}Zr_{0.2}Ta_{0.2}Nb_{0.2}Ti_{0.2})C$ with binary carbides HfC, ZrC, TaC, NbC and TiC. The data is at room temperature unless specifically indicated.

| Materials | Thermal diffusivity, $\alpha$ (mm$^2$/s) | Specific heat capacity, $c_p$ (J/kg·K) | Thermal conductivity, $k$ (W/m·K) | Thermal expansion coefficient, $\alpha_L$ ($10^{-6}$ K$^{-1}$) |
|---|---|---|---|---|
| **$(Hf_{0.2}Zr_{0.2}Ta_{0.2}Nb_{0.2}Ti_{0.2})C$** | 4.6 (29.5 °C)<br>3.68 (50.7 °C)<br>3.73 (70.8 °C) | 191 (29.5 °C)<br>161 (50.7 °C)<br>155 (70.8 °C) | 6.45 (29.5 °C)<br>5.56 (50.7 °C)<br>5.42 (70.8 °C) | 6.44 (25 °C) |
| HfC | 12.3 | 188 | 29.3 | 6.6[19] |

| | | | | |
|---|---|---|---|---|
| ZrC | 15.2 | 368 | 33.5 | 6.74[20] |
| TaC | 12.4 | 356 | 33.5 | 6.29[20] |
| NbC | 6.29 | 569 | 6.3 | 6.65[20] |
| TiC | 8.32 | 190 | 22.2 | 6.99[20] |

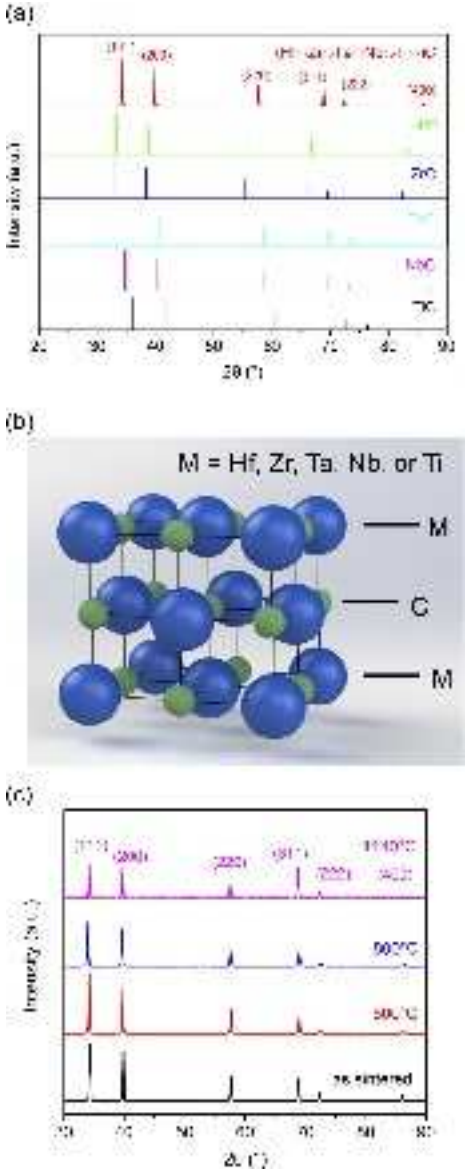


jace_15779_f1.tiff

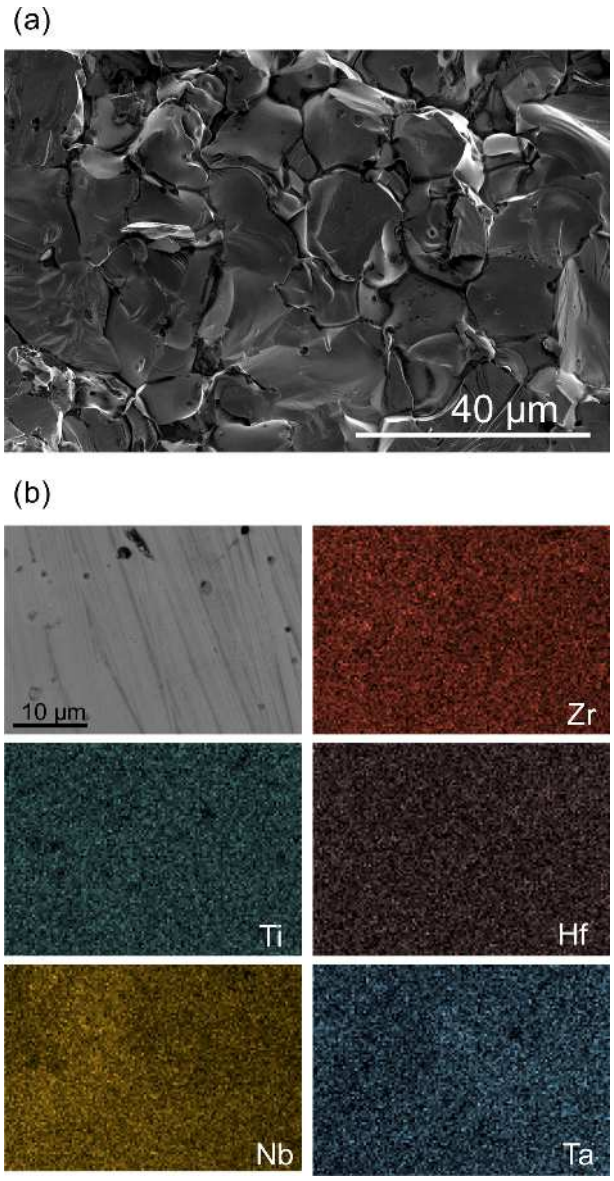


jace_15779_f2.tif